

Superconducting persistent-current qubit

T. P. Orlando

Department of Electrical Engineering and Computer Science, MIT, Cambridge, Massachusetts 02139

J. E. Mooij

*Department of Electrical Engineering and Computer Science, MIT, Cambridge, Massachusetts 02139
and Department of Applied Physics, Delft University of Technology, P.O. Box 5046, 2628 CJ Delft, The Netherlands*

Lin Tian

Department of Physics, MIT, Cambridge, Massachusetts 02139

Caspar H. van der Wal

Department of Applied Physics, Delft University of Technology, P.O. Box 5046, 2628 CJ Delft, The Netherlands

L. S. Levitov

Department of Physics and Center for Material Science and Engineering, MIT, Cambridge, Massachusetts 02139

Seth Lloyd

Department of Mechanical Engineering, MIT, Cambridge, Massachusetts 02139

J. J. Mazo

*Department of Electrical Engineering and Computer Science, MIT, Cambridge, Massachusetts 02139
and Departamento de Física de la Materia Condensada and ICMA, CSIC-Universidad de Zaragoza, E-50009 Zaragoza, Spain
(Received 13 July 1999)*

We present the design of a superconducting qubit that has circulating currents of opposite sign as its two states. The circuit consists of three nanoscale aluminum Josephson junctions connected in a superconducting loop and controlled by magnetic fields. The advantages of this qubit are that it can be made insensitive to background charges in the substrate, the flux in the two states can be detected with a superconducting quantum interference device, and the states can be manipulated with magnetic fields. Coupled systems of qubits are also discussed as well as sources of decoherence. [S0163-1829(99)00746-8]

I. INTRODUCTION

Quantum computers are devices that store information on quantum variables such as spins, photons, and atoms, and that process that information by making those variables interact in a way that preserves quantum coherence.¹⁻⁵ Typically, these variables consist of two-state quantum systems called quantum bits or “qubits.”⁶ To perform a quantum computation, one must be able to prepare qubits in a desired initial state, coherently manipulate superpositions of a qubit’s two states, couple qubits together, measure their state, and keep them relatively free from interactions that induce noise and decoherence.^{1-4,7,8} Qubits have been physically implemented in a variety of systems, including cavity quantum electrodynamics,⁹ ion traps,¹⁰ and nuclear spins.^{11,12} Essentially any two-state quantum system that can be addressed, controlled, measured, coupled to its neighbors, and decoupled from the environment, is potentially useful for quantum computation and quantum communications.^{13,14} Electrical systems that can be produced by modern lithography, such as nanoscaled quantum dots and tunnel junctions, are attractive candidates for constructing qubits: a wide variety of potential designs for qubits and their couplings are available, and the qubits are easily scaled to large arrays that can be integrated in electronic circuits.^{3,15} For this reason, mesoscopic superconducting circuits of ultrasmall Josephson

junctions have been proposed as qubits¹⁶⁻²⁰ and we detail one such circuit in this paper.

Compared with the photonic, atomic, and nuclear qubits already constructed, solid-state proposals based on lithography such as the one described here have two considerable disadvantages and one considerable advantage. The first disadvantage is noise and decoherence:^{3,7,8} the solid-state environment has a higher density of states and is typically more strongly coupled to the degrees of freedom that make up the qubit than is the environment for photons in cavities, ions in ion traps, and nuclear spins in a molecule or crystal. Extra care must be taken in solid state to decouple the qubit from all sources of noise and decoherence in its environment. The second disadvantage is manufacturing variability:⁸ each ion in an ion trap is identical by nature, while each lithographed Josephson junction in an integrated circuit will have slightly different properties. Solid-state designs must either be insensitive to variations induced by the manufacturing process, or must include a calibration step in which the parameters of different subcircuits are measured and compensated for.¹⁵

The advantage of solid state lithographed circuits is their flexibility: the layout of the circuit of Josephson junctions or quantum dots is determined by the designer, and its parameters can be adjusted continuously over a wide range. As the results presented in this paper demonstrate, this flexibility allows the design of circuits in which the variables that reg-

ister the qubits are only weakly coupled to their environment. In addition, the flexibility in circuit layout allows many possible options for coupling qubits together, and for calibrating and adjusting the qubits' parameters. That is, the advantage of flexibility in design can compensate for the disadvantages of decoherence and manufacturing variability.

The flexibility in design afforded by lithography conveys a further advantage to constructing quantum computers. As noted above, a qubit has to accomplish at least five functions: it has to be addressed, controled, measured, coupled to its neighbors, and decoupled from the environment. One of the axioms of design is that the number of parameters that characterize a system's design should be at least as great as the number of parameters that characterize the system's function.²¹ The problem of having too few design parameters available is particularly acute in the design of quantum computers and qubits: a quantum computer is a device in which a number of physical degrees of freedom are used to register information and to perform the computation. Degrees of freedom that are not used to compute are sources of noise and must be isolated from the computing degrees of freedom. Designs for quantum computers are accordingly more constrained by fundamental physics than are designs for conventional computers: if one is storing information on a cesium atom, then the "design parameters" of the cesium atom—its energy levels, decoherence times, interaction strengths, etc.—are fixed by nature once and for all. In the lithographed Josephson junction circuits proposed here, by contrast, it is possible to make qubits that have a variety of different design parameters, each of which can be adjusted to optimize different functions.

II. JOSEPHSON-JUNCTION QUBITS

The superconducting Josephson tunnel junction is described by a critical current I_0 and a capacitance C . (We will assume that the resistive channel of the junction is negligibly small.) For superconducting circuits the geometrical loop inductance L_s is also important if $\Lambda = L_J/L_s < 1$, where $L_J = \Phi_0/2\pi I_0$ is the inductance associated with a Josephson junction in the loop. Here $\Phi_0 = h/2e$ is the superconducting flux quantum. Josephson circuits can be divided into two general categories. Circuits of the first type have $\Lambda \gg 1$ so that the induced flux in the loop is not important. These circuits are typically made of aluminum, and the mesoscopic nature of their electronic transport has been studied in nanoscaled circuits. Circuits of the second type have $\Lambda \ll 1$, and induced flux caused by circulating currents is important. These circuits are typically made of niobium, and the macroscopic nature of the tunneling of flux has been studied in small-scaled circuits.

The prospects of using superconducting circuits of the first type as qubits is encouraging because extensive experimental and theoretical work has already been done on mesoscopic superconducting circuits. (For a review of this work see Chap. 7 in Ref. 22 and in Ref. 23.) In circuits of the first type ($\Lambda \gg 1$), two energy scales determine the quantum-mechanical behavior: The Josephson coupling energy, $E_J = I_0\Phi_0/2\pi$, and the coulomb energy for single charges, $E_c = e^2/2C$. The energies can be determined by the phases of the Cooper pair wave function of the nodes (islands) and the

number of excess Cooper pairs on each node. The phase and the number can be expressed as quantum-mechanical conjugate variables.²⁴

In the "superconducting" limit $E_J > E_c$, the phase is well defined and the charge fluctuates. In the "charging" limit, the charges on the nodes are well defined and the phase fluctuates strongly. When E_J and E_c are within a few orders of magnitude of each other, the eigenstates must be considered as quantum-mechanical superpositions of either charge states or phase states. Such superposition states are important in designing qubits. Experimental studies have been performed by several groups with aluminum tunnel junctions with dimensions below 100 nm.^{22,23} Superposition of charge states in circuits in the charging regime have been demonstrated^{25–27} and are in quantitative agreement with theory.^{28,29} The Heisenberg uncertainty principle has been demonstrated when $E_J \approx E_c$.^{30,26} When $E_J > E_c$ topological excitations known as vortices exists and quantum mechanical interference of these quantities has been observed.³¹ Unfortunately circuits of the first type in the charging regime are sensitive to fluctuating off-set charges that are present in the substrate.^{32,33} These random offset charges make difficult the design of a controllable array of quantum circuits and introduce a strong source of decoherence.

In circuits of the second type ($\Lambda \ll 1$), the quantum variables can be related to the flux in the loops and their time derivatives. For a superconducting loop with a single Josephson junction, known as an rf superconducting quantum interference device (SQUID), thermal activation of macroscopic quantum states³⁴ has been observed as well as macroscopic quantum tunneling between states and the discrete nature of the quantum states.³⁵ One of the advantages of these rf SQUID systems is that the two states have circulating currents of opposite sign and, hence, produce a readily measurable flux of opposite signs. To date no superposition of states have been demonstrated in the niobium circuits, although the improving quality of the niobium tunnel junctions may allow such a demonstration.^{36,37}

The goal of this paper is to design a qubit using circuits of the first type with aluminum, yet to have states (like in circuits of the second type) that are circulating currents of opposite sign. These circulating current states create a magnetic flux of about $10^{-3}\Phi_0$ and we refer to these as "persistent current (PC) states." These states obey all five functional requirements for a quantum bit: (1) The superconducting circuit is at a sufficiently low temperature that the PC states can easily be prepared in their ground state. (2) The PC states can be manipulated precisely with magnetic fields. (3) Two qubits can be readily coupled inductively, and the inductive coupling can be turned on and off. (4) The flux of the PC states can be detected and measured using a SQUID-type detector. (5) In contrast with charge quantum states in Josephson circuits, the PC can be made insensitive to background charges and effectively decoupled from their electrostatic environment. The magnetic coupling to the PC states and the environment can also be made sufficiently weak.

III. THE CIRCUIT

The circuit of the qubit is shown in Fig. 1. Each junction is marked by an \times and is modeled^{22,38} by a parallel combi-

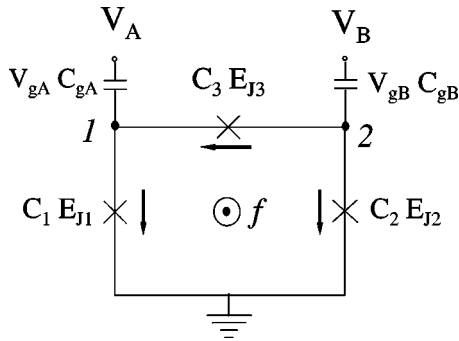


FIG. 1. The three-junction qubit. Josephson junctions 1 and 2 both have Josephson energies E_J and capacitance C and Josephson junction 3 has a Josephson energy and capacitance α times larger. The nodes 1 and 2 represent the superconducting islands (nodes) that are coupled by gate capacitors $C_g = \gamma C$ to gate voltages V_A and V_B . The arrows define the direction of the currents. The flux is taken out of the page.

nation of an ideal Josephson junction and a capacitor C_i . The parallel resistive channel is assumed negligible. The ideal Josephson junction has a current-phase relation, $I_i = I_0 \sin \varphi_i$ where φ_i , is the gauge-invariant phase of junction i .

For the calculation of the energy the inductance of the loop is considered negligible, $\Lambda \gg 1$, so that the total flux is the external flux. In this case, fluxoid quantization around the loop containing the junctions gives $\varphi_1 - \varphi_2 + \varphi_3 = -2\pi f$. Here f is the magnetic frustration and is the amount of external magnetic flux in the loop in units of the flux quantum Φ_0 .

The Josephson energy due to each junction is $E_{Jn}(1 - \cos \varphi_n)$. The total Josephson energy U is then $U = \sum_i E_{Ji}(1 - \cos \varphi_i)$. Combined with the flux quantization condition the Josephson energy is³⁹

$$\frac{U}{E_J} = 2 + \alpha - \cos \varphi_1 - \cos \varphi_2 - \alpha \cos(2\pi f + \varphi_1 - \varphi_2). \quad (1)$$

The important feature of this Josephson energy is that it is a function of two phases.⁴⁰ For a range of magnetic frustration f , these two phases, φ_1 and φ_2 , permit two stable configurations, which correspond to dc currents flowing in opposite directions. We illustrate this in Fig. 2, where we plot the energy of the minimum of the system as a function of f for $\alpha=0.8$.

The energy is periodic with period $f=1$ and is symmetric about $f=1/2$. Near $f=1/2$, there is a region $[1/2 - f_c, 1/2 + f_c]$ where there are two stable solutions. The inset plots f_c as a function of α . These two solutions have circulating currents of opposite direction and are degenerate at $f=1/2$. The calculation of the energy for the stable solutions and f_c is given in Appendix A.

The main feature of the qubit that is proposed in this paper is to use these two states of opposite current as the two states of the qubit. By adding the charging energy (the capacitive energy) of the junctions and considering the circuit quantum mechanically, we can adjust the parameters of the circuit so that the two lowest states of the system near $f=1/2$ will correspond to these two classical states of opposite circulating currents. Moreover, we will show that these two

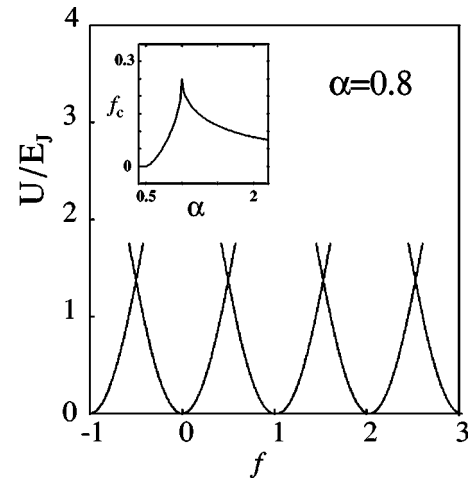


FIG. 2. U/E_J vs f for $\alpha=0.8$ and for minimum energy phase configuration. The energy is periodic with period $f=1$ and is symmetric about $f=1/2$. Near $f=1/2$, there is a region $[1/2 - f_c, 1/2 + f_c]$ where there are two stable solutions. The inset plots f_c as a function of α .

states can be made insensitive to the gate voltages and the random offset charges. The quantum mechanics of the circuit will be considered in detail in the next section.

The stable classical solutions correspond to energy minima in $U(\varphi_1, \varphi_2)$. Let us consider the case of $f=1/2$. For $\alpha \leq 1/2$, U has only one minimum at $\varphi_1 = \varphi_2 = 0 \pmod{2\pi}$. Above the critical value of $\alpha=1/2$, this minimum bifurcates into two degenerate minima at $\varphi_1 = -\varphi_2 = \pm \varphi^* \pmod{2\pi}$ where $\cos \varphi^* = 1/2\alpha$. The minima form a two-dimensional pattern with the two minima at $(\varphi^*, -\varphi^*)$ and $(-\varphi^*, \varphi^*)$ repeated in a two-dimensional square lattice. This pattern can be seen in Fig. 3, which is a contour plot of the Josephson energy as a function of the phase variables for $\alpha=0.8$. The nested nearly circular contours mark the maxima in the potential. The figure-eight-shaped contour encloses two minima.

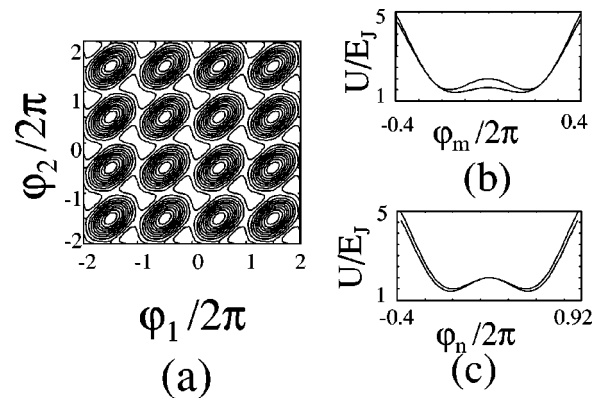


FIG. 3. (a) A contour plot of the Josephson energy (potential energy) $U(\varphi_1, \varphi_2)$ for $f=1/2$ for $\alpha=0.8$. The nested nearly circular shapes mark the maxima in the potential, and the figure-eight-shaped contours enclose two minima. (b) a plot of the potential vs φ_m , the phase along the direction between these two minimum in the same unit cell, (c) a plot of the potential vs φ_n , the phase along direction from one minima to its next-nearest neighbor. Note that the barrier is a saddle point. The upper curve in each figure is for $\alpha=1.0$ and the lower for $\alpha=0.8$.

Figure 3(b) shows the potential along φ_m , between the two minima in a unit cell; that is, along the line $\varphi_2 = -\varphi_1$. The upper curve is for $\alpha = 1.0$ and the lower for $\alpha = 0.8$. Figure 3(c) shows the potential vs φ_n , which connects one minimum [say at $(-\varphi^*, \varphi^*)$] to its next-nearest neighbor [at $(\varphi^*, 2\pi - \varphi^*)$]. For $\alpha = 0.8$ the energy barrier between the two minima is much lower than the energy barrier from the minimum in one unit cell to the neighboring unit cell. For $\alpha = 1.0$ the energy barrier from unit cell to unit cell is nearly the same as the barrier within the unit cell. The ability to manipulate the potential landscape by changing α will be important in designing the qubit.

We now consider the electric energy T stored in the five capacitors in the circuit. Each capacitor C_j has a voltage across it of V_j so that

$$T = \frac{1}{2} \sum_j C_j V_j^2 - Q_{gA} V_A - Q_{gB} V_B. \quad (2)$$

Here $j = 1, 2, 3$, and gA and gB . The last two terms subtract the work done by the voltage source to give the available electric (free) energy.⁴¹ The voltage across each Josephson junction is given by the Josephson voltage-phase relation $V_n = (\Phi_0/2\pi) \dot{\varphi}_n$, where the over-dot indicates a partial time derivative. The ground in the circuit labels the zero of potential and is a virtual ground.

The voltage across the gate capacitor gA is $V_{gA} = V_A - V_1$ and similarly for $V_{gB} = V_B - V_2$. The electric energy can then be written in terms of the time derivatives of the phases as

$$T = \frac{1}{2} \left(\frac{\Phi_0}{2\pi} \right)^2 \dot{\vec{\varphi}}^T \cdot \mathbf{C} \cdot \dot{\vec{\varphi}}. \quad (3)$$

The constant term $-\frac{1}{2} \vec{V}_g^T \cdot \mathbf{C}_g \cdot \vec{V}_g$ has been neglected and

$$\dot{\vec{\varphi}} = \begin{pmatrix} \dot{\varphi}_1 \\ \dot{\varphi}_2 \end{pmatrix}, \quad \mathbf{C} = C \begin{pmatrix} 1 + \alpha + \gamma & -\alpha \\ -\alpha & 1 + \alpha + \gamma \end{pmatrix}, \quad (4)$$

and

$$\vec{V}_g = \begin{pmatrix} V_A \\ V_B \end{pmatrix}, \quad \mathbf{C}_g = \gamma C \begin{pmatrix} 1 & 0 \\ 0 & 1 \end{pmatrix}. \quad (5)$$

The classical equations of motion can be found from the Lagrangian $\mathcal{L} = T - U$. We take the electrical energy as the kinetic energy and the Josephson energy as the potential energy.⁴² The canonical momenta is $P_i = \partial \mathcal{L} / \partial \dot{\varphi}_i$. To attach a more physical meaning to the canonical momentum, we shift the Lagrangian by a Galilean-like transformation to

$$\mathcal{L} = T - U - \left(\frac{\Phi_0}{2\pi} \right)^2 \dot{\vec{\varphi}}^T \cdot \mathbf{C}_g \cdot \vec{V}_g. \quad (6)$$

The canonical momentum is then

$$\vec{P} = \left(\frac{\Phi_0}{2\pi} \right)^2 \mathbf{C} \cdot \dot{\vec{\varphi}} - \left(\frac{\Phi_0}{2\pi} \right) \mathbf{C}_g \cdot \vec{V}_g \quad (7)$$

and is directly proportional to the charges at the islands at nodes 1 and 2 in Fig. 1 as

$$\vec{Q} = \frac{2\pi}{\Phi_0} \vec{P}. \quad (8)$$

[For any Josephson circuit it can be shown that there exist linear combinations of the phases across the junctions such that these linear combination can be associated with each node and the corresponding conjugate variable is proportional to the charge at that node.^{43,44} If self and mutual inductances need to be included in the circuit (as we argue does not need to be done in our case), then additional conjugate pairs would needed.]⁴⁴

The classical Hamiltonian, $H = \sum_i P_i \dot{\varphi}_i - \mathcal{L}$, is

$$H = \frac{1}{2} \left(\vec{P} + \frac{\Phi_0}{2\pi} \vec{Q}_g \right)^T \cdot \mathbf{M}^{-1} \cdot \left(\vec{P} + \frac{\Phi_0}{2\pi} \vec{Q}_g \right) + U(\vec{\varphi}), \quad (9)$$

where the effective mass $\mathbf{M} = (\Phi_0/2\pi)^2 \mathbf{C}$ is anisotropic and the induced charge on the island is $\vec{Q}_g = \mathbf{C}_g \cdot \vec{V}_g$. When driven by an additional external current source, the classical dynamics of this system have been studied in recent years both theoretically^{45,46} and experimentally.^{47,48}

Note that the kinetic energy part of this Hamiltonian is

$$T = \frac{1}{2} (\vec{Q} + \vec{Q}_g)^T \cdot \mathbf{C}^{-1} \cdot (\vec{Q} + \vec{Q}_g), \quad (10)$$

which is just the electrostatic energy written in terms of the charges and induced charges on the islands. Often this is the method used in discussing the charging part of the Hamiltonian. See, for example, Ref. 43 and the references therein. A characteristic charge is e and characteristic capacitance is C so that the characteristic electric energy is the so-called charging energy, $E_c = e^2/2C$.

IV. QUANTUM CIRCUIT

The transition to treating the circuit quantum mechanically is to consider the classically conjugate variables in the classical Hamiltonian as quantum-mechanical operators.^{49,50} For example, the momenta can be written as $P_1 = -i\hbar \partial / \partial \varphi_1$ and $P_2 = -i\hbar \partial / \partial \varphi_2$ and the wave function can then be considered as $|\Psi\rangle = \Psi(\varphi_1, \varphi_2)$.

In this representation the plane-wave solutions, such as $\psi = \exp\{-i(l_1\varphi_1 + l_2\varphi_2)\}$ correspond to a state that has l_1 Cooper pairs on island (node) 1 and l_2 Cooper pairs on island 2. These plane-wave states are the so-called charging states of the system.^{51,28} Since a single measurement of the number of Cooper pairs on each island must be an integer, then so should the l 's here. (Note the expectation value of the number of Cooper pairs is not restricted to an integer.) Furthermore, an eigenfunction $\Psi(\varphi_1, \varphi_2)$ can be written as a weighted linear combination of these charge states. This means that $\Psi(\varphi_1, \varphi_2)$ is periodic when each of the phases are changed by 2π , as in the physical pendulum.⁵²

By considering $\Psi(\varphi_1, \varphi_2) = \exp\{i(k'_1\varphi_1 + k'_2\varphi_2)\} \chi(\varphi_1, \varphi_2)$ with $[k'_1, k'_2] = -(\gamma C/2e)[V_A, V_B]$, the Hamiltonian for $\chi(\varphi_1, \varphi_2)$ is almost the same but the induced charges are now transformed out of the problem, and we refer to this new Hamiltonian as the transformed Hamiltonian H_t , where⁵³

$$H_t = \frac{1}{2} \vec{P}^T \cdot \mathbf{M}^{-1} \cdot \vec{P} + E_J \{ 2 + \alpha - \cos \varphi_1 - \cos \varphi_2 - \alpha \cos(2\pi f + \varphi_1 - \varphi_2) \}. \quad (11)$$

The resulting equation $H_t \chi(\varphi_1, \varphi_2) = E \chi(\varphi_1, \varphi_2)$ is the same as for an anisotropic, two-dimensional particle in the periodic potential U . The solutions are Bloch waves with the ‘‘crystal momentum’’ \mathbf{k} values corresponding to $-\mathbf{k}'$, which is proportional to the applied voltages. This choice of crystal momentum ensures that $\Psi(\varphi_1, \varphi_2)$ is periodic in the phases.

We will first present the numerical results of the energy levels and wave functions for the circuit. Then we will use the tight-binding-like approximation to understand the results semiquantitatively.

The eigenvalues and eigen-wave-functions for the transformed Hamiltonian H_t are solved numerically by expanding the wave functions in terms of states of constant charge or states of constant phase. The states of constant charge result in the central equation for Bloch functions (see Ref. 74) and are computationally efficient when $E_c > E_J$. The states of constant phase are solved by putting the phases on a discrete lattice and the numerics are more efficient when $E_J > E_c$. Since the Josephson energy dominates, we will show results computed using the constant phase states. (However, when we used the constant charge states, we obtained the same results.)

The numerical calculations are done in a rotated coordinate system, which diagonalizes the capacitance matrix \mathbf{C} by choosing as coordinates the sum and difference of the phases, $\varphi_p = (\varphi_1 + \varphi_2)/2$ and $\varphi_m = (\varphi_1 - \varphi_2)/2$. The resulting reduced Hamiltonian is

$$H_t = \frac{1}{2} \frac{P_p^2}{M_p} + \frac{1}{2} \frac{P_m^2}{M_m} + E_J \{ 2 + \alpha - 2 \cos \varphi_p \cos \varphi_m - \alpha \cos(2\pi f + 2\varphi_m) \}, \quad (12)$$

where the momenta can be written as $P_p = -i\hbar \partial / \partial \varphi_p$ and $P_m = -i\hbar \partial / \partial \varphi_m$. The mass terms are $M_p = (\Phi_0 / 2\pi)^2 2C(1 + \gamma)$ and $M_m = (\Phi_0 / 2\pi)^2 2C(1 + 2\alpha + \gamma)$. In this coordinate system the full wave function $\Psi(\varphi_p, \varphi_m) = \exp\{i(k'_p \varphi_p + k'_m \varphi_m)\} \chi(\varphi_p, \varphi_m)$ with $[k'_p, k'_m] = -(\gamma C / 2e)[V_A + V_B, V_A - V_B]$ and $H_t \chi(\varphi_p, \varphi_m) = E \chi(\varphi_p, \varphi_m)$. Also the two minima of the potential $U(\varphi_p, \varphi_m)$ within a unit cell form a periodic two-dimensional centered cubic lattice with lattice constants $\mathbf{a}_1 = 2\pi \mathbf{i}_x$ and $\mathbf{a}_2 = \pi \mathbf{i}_x + \pi \mathbf{i}_y$.

Figure 4 shows the energy levels as a function of f and as a function of the gate voltage, which is given in terms of \mathbf{k} . We have taken $E_J/E_c = 80$, $\alpha = 0.8$, and $\gamma = 0.02$ in this example. The energy levels are symmetric about $f = 1/2$. In Fig. 4(a), we see that the two lowest energy levels near $f = 1/2$ have opposite slopes, indicating that the circulating currents are of opposite sign. We also see that there is only a small range of $0.485 < f < 0.5$, where the qubit can be operated between these states of opposite circulating current. This range is consistent with the range $[\frac{1}{2} \pm f_c]$ from the classical stability as shown in Fig. 2. At $f = 0.49$ direct calculation of the average circulating current, $\langle \Psi | I_0 \sin \varphi_1 | \Psi \rangle$ gives that the circulating current for the lower level is $I_1/I_0 = -0.70$ and for the upper level is $I_2/I_0 = +0.70$. (A calculation of

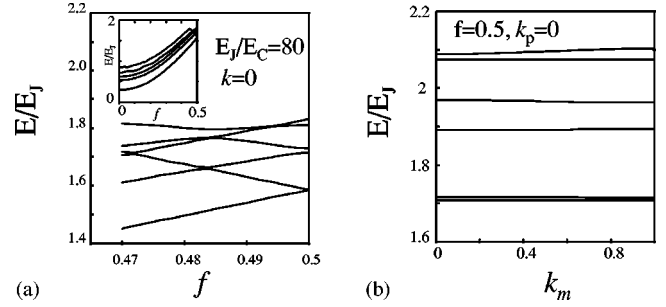


FIG. 4. The energy levels E vs frustration and gate voltage for $E_J/E_c = 80$, $\alpha = 0.8$, and $\gamma = 0.02$. The gate voltage is related to the \mathbf{k} values by $[k_p, k_m] = (\gamma C / 2e)[V_A + V_B, V_A - V_B]$, (a) E/E_J vs f_b near $f_b = 1/2$ for $[k_p, k_m] = [0, 0]$, and (b) E/E_J vs k_m for $k_p = 0$.

the circulating current from the thermodynamic relation $-\Phi_0^{-1} \partial E_n / \partial f$ gives the same result.) For a loop of diameter of $d = 10 \mu\text{m}$, the loop inductance is of the order $\mu_0 d \approx 10 \text{ pH}$.⁵⁴ For $I_0 \approx 400 \text{ nA}$ ($E_J = 200 \text{ GHz}$), the flux due to the circulating current is $LI I_0 \approx 10^{-3} \Phi_0$, which is detectable by an external SQUID. Nevertheless, the induced flux is small enough that we are justified in neglecting its effect when calculating the energy levels.

The difference in energy between the lower and upper level at the operating point of $f = 0.485$ is about $0.1 E_J \approx 20 \text{ GHz}$. Moreover, Fig. 4(b) shows that the energies of these levels is very insensitive to the gate voltages, or equivalently, to the random offset charges. The numerical results show that the bands are flat to better than one part in a thousand, especially at $f = 0.48$. To understand the underlying physics, a tight-binding model is developed.

Tight-binding model

Consider the case near the degeneracy point $f = 1/2$. The minima in energy occur when $\varphi_p^* = 0$ and $\varphi_m = \pm \varphi_m^*$, where $\cos \varphi_m^* = 1/2\alpha$. Near the minimum at $[\varphi_m, \varphi_p] = [\varphi_m^*, 0]$, the potential looks like a double potential well repeated at lattice points $\mathbf{a}_1 = 2\pi \mathbf{i}_x$ and $\mathbf{a}_2 = \pi \mathbf{i}_x + \pi \mathbf{i}_y$. Figure 5 shows the two eigenfunctions in a unit cell.

The wave function for the lower level (Ψ_1) is symmetric and the wave function for the upper level (Ψ_2) is antisymmetric. Both of the wave functions are localized near the two minima in U in the unit cell.

To find an approximate tight-binding solution, let $u(\varphi_m, \varphi_p)$ be the wave function for the ground state on one

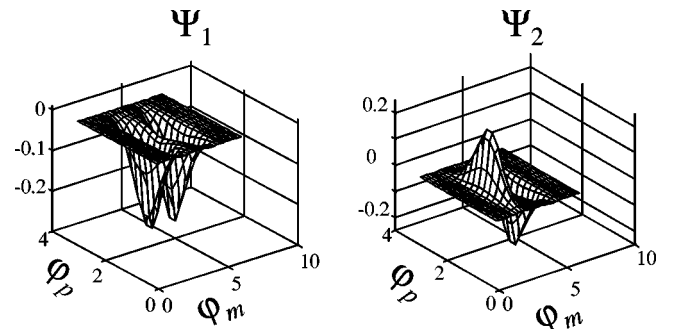


FIG. 5. The eigen-wave-functions for the lower (Ψ_1) and upper (Ψ_2) energy levels at $f = 1/2$ as a function of the phases.

side of the double potential wells, and $v(\varphi_m, \varphi_p)$ be the wave function on the other side. The tight-binding solution for H_t in Eq. (12) is $\Phi = c_u u + c_v v$ and satisfies

$$\begin{pmatrix} H_{uu} & H_{uv} \\ H_{vu} & H_{vv} \end{pmatrix} \begin{pmatrix} c_u \\ c_v \end{pmatrix} = E \begin{pmatrix} c_u \\ c_v \end{pmatrix}. \quad (13)$$

Because the double well is symmetric at $f=1/2$, each wave function has the same energy ϵ_0 and so $H_{uu}=H_{vv}=\epsilon_0$. Let t_1 be the tunneling matrix element between these two minima in the same unit cell and t_2 between nearest-neighbor minima in the adjacent unit cells. Then $H_{uv}=H_{vu}^* = -t_1 - t_2 e^{ik \cdot a_2} - t_2 e^{ik \cdot (a_1 - a_2)}$. The eigen-energy-levels are $E = \epsilon_0 \mp |H_{uv}|$. The effect of t_1 is to split the degeneracy of the two states so that at $k=0$, the energy is $\epsilon_0 \mp (2t_2 + t_1)$ for the symmetric and antisymmetric states respectively. The effect of t_2 is to give dispersion in k , that is, in gate voltage and offset charges, to the energy levels. Because we want to minimize the gate-voltage (and offset charge) dependence, we seek to minimize the tunneling t_2 from one unit cell to another. Likewise, we want the two localized states in the two wells to interact, so that we want t_1 to be nonzero. This is why the potential landscape in Fig. 3 was chosen to have $\alpha \approx 0.8$: The potential has a much lower barrier between states in the double well, but a large barrier between states from one double well to the next.

An estimate of t_i can be obtained by the WKB method, from calculating the action S_i between the two minima and using $t_i \approx (\hbar \omega_i / 2\pi) e^{-S_i/\hbar}$ where ω_i is the attempt frequency of escape in the potential well. The action from point $\vec{\varphi}_a$ to $\vec{\varphi}_b$ is

$$S = \int_{\vec{\varphi}_a}^{\vec{\varphi}_b} [2M_{nn}(E-U)]^{1/2} |d\varphi_n|. \quad (14)$$

Here \mathbf{n} is a unit vector along the path of integration, $d\varphi_n$ the differential path length, and $M_{nn} = \mathbf{n}^T \cdot \mathbf{M} \cdot \mathbf{n}$ is the component of the mass tensor along the path direction. In Eq. (14) we will approximate the energy difference $E-U$ which measures the deviation in the potential energy ΔU from the minima along the path.

First, consider the calculation of t_1 , the tunneling matrix element within the unit cell. The path of integration is taken from $(-\varphi_m^*, 0)$ to $(\varphi_m^*, 0)$ along the direction $\mathbf{n} = \mathbf{i}_x$, so that $M_{nn} = M_m$ for this path. The potential energy at the minima is $U_{min} = 2 - 1/2\alpha$. The difference in the potential energy from the minima at $(-\varphi_m^*, 0)$ along this path can be written as $\Delta U_1 = E_J \{2\alpha(\cos \varphi_m - 1/2\alpha)^2\}$. The action along this path is then

$$S_1 = \int_{-\varphi_m^*}^{\varphi_m^*} (4M_m \alpha E_J)^{1/2} \left(\cos \varphi_m - \frac{1}{2\alpha} \right) d\varphi_m, \quad (15)$$

which yields

$$S_1 = \hbar [4\alpha(1+2\alpha+\gamma)E_J/E_c]^{1/2} \left(\sin \varphi_m^* - \frac{1}{2\alpha} \varphi_m^* \right). \quad (16)$$

Now consider t_2 , the tunneling from unit cell to unit cell. For example, take the integration to be from $(\varphi_m^*, 0)$ to one of

its nearest-neighbor minima at $(\pi - \varphi_m^*, \pi)$. We will take the path of integration to be a straight line joining these two points in the φ_m - φ_p plane. This path is not the optimal trajectory, but the difference in the action for this straight line path from the optimal trajectory is quadratic in the small deviations of these two paths. The straight line path is described by $\varphi_m = \varphi_m^* + \lambda \varphi_p$, where $\lambda = (\pi - 2\varphi_m^*)/\pi$; it has a direction of $\mathbf{n} = \lambda \mathbf{i}_x + \mathbf{i}_y$ and a path length of $ds = \sqrt{1+\lambda^2} d\varphi_p$. The mass on this direction is $M_2 = (M_p + \lambda^2 M_m)/(1+\lambda^2)$. The difference of the potential energy along this path from the minima energy is $\Delta U_2/E_J = -2 \cos \varphi_p \cos(\varphi_m^* + \lambda \varphi_p) + 2\alpha \cos^2(\varphi_m^* + \lambda \varphi_p) + 1/2\alpha$. The action is then

$$S_2 = [2M_2 E_J (1+\lambda^2)]^{1/2} \int_0^\pi \left(\frac{\Delta U_2}{E_J} \right)^{1/2} d\varphi_p. \quad (17)$$

The integrand is not analytically integrable, but being zero at the end points of the integration, it is well approximated by $\sqrt{\Delta U_2/E_J} \approx (1/\sqrt{2\alpha}) \cos(\varphi_p - \pi/2)$. With this approximation, $S_2 = (4M_2 E_J (1+\lambda^2)/\alpha)^{1/2}$, which is

$$S_2 = \hbar \sqrt{\frac{E_J}{E_c} \left(\frac{(1+\gamma)(1+\lambda^2)}{\alpha} + 2\lambda^2 \right)}. \quad (18)$$

To compare the tunneling rates we would first need the attempt frequencies in the two directions. However, we can consider the attempt frequencies to be of the same order of magnitude and thus $t_2/t_1 \sim e^{-(S_2 - S_1)/\hbar}$. For $\alpha = 0.8$, we find that $S_1/(\hbar \sqrt{E_J/E_c}) \approx 0.6$ and $S_2/(\hbar \sqrt{E_J/E_c}) \approx 1.4$. For $E_J/E_c \sim 100$, then $t_2/t_1 \sim 10^{-4} \ll 1$. We are therefore able to ignore t_2 , the tunneling from the unit cell to unit cell. This means that there is little dispersion in the energy levels with \mathbf{k} and, consequently, with the voltage or offset charges. In fact, using the action one can show that for α smaller than about 0.85, $t_1 > t_2$ for $E_J/E_c \approx 80$. Throughout the rest of the paper we will choose parameters so that the effects of t_2 can be ignored.

We now obtain an approximate solution for the energy levels and tunneling matrix elements by modeling each side of the double potential. Near the minimum at $[\varphi_m, \varphi_p] = [\varphi_m^*, 0]$, the potential looks like an anisotropic two-dimensional harmonic oscillator. The Hamiltonian in the vicinity of the minimum is approximately (with $\vec{Q}_g = 0$)

$$\begin{aligned} \mathcal{H} \approx & \frac{1}{2} \frac{P_p^2}{M_p} + \frac{1}{2} M_p \omega_p^2 \varphi_p^2 + \frac{1}{2} \frac{P_m^2}{M_m} \\ & + \frac{1}{2} M_m \omega_m^2 (\varphi_m - \varphi_m^*)^2 + U_0, \end{aligned} \quad (19)$$

where

$$\frac{\hbar \omega_p}{E_J} = \sqrt{\frac{4}{\alpha(1+\gamma)(E_J/E_c)}} \quad (20)$$

and

$$\frac{\hbar \omega_m}{E_J} = \sqrt{\frac{4(4\alpha^2 - 1)}{\alpha(1+2\alpha+\gamma)(E_J/E_c)}} \quad (21)$$

and $U_0 = 2 - 1/2\alpha$. The ground state ϕ_0 of the single harmonic well has energy $\epsilon_0 = \hbar(\omega_p + \omega_m)/2 + U_0$. Let us now

TABLE I. A comparison of the energy levels with the approximate harmonic oscillator levels (with harmonic and anharmonic terms) with the numerical calculations. Here $f=1/2$, $\alpha=0.8$, $\gamma=0.02$, and $E_J/E_c=80$. Also, $U_0=1.38$ and $U_{\text{bar}}=0.225$ for the harmonic and anharmonic estimations. All the energies are in units of E_J .

	$\hbar\omega_m$	$\hbar\omega_p$	E_0	$(E_1+E_2)/2$	$(E_3+E_4)/2$
Harmonic	0.193	0.247	1.60	1.79	1.84
Anharmonic	0.183	0.238	1.59	1.77	1.83
Numerical	0.154	0.226	1.58	1.74	1.81

use this approximation to understand the energy levels, first at $f=1/2$ and then near this point.

At $f=1/2$ we expect the four lowest energy levels of the two-dimensional harmonic oscillator to be with $\omega_m < \omega_p$, $E_1 = \epsilon_0 - t_1$, $E_2 = \epsilon_0 + t_1$, $E_3 = \epsilon_0 - t_1 + \hbar\omega_m$, and $E_4 = \epsilon_0 + t_1 + \hbar\omega_m$. Table I compares the results and we also list the small anharmonic corrections to the simple harmonic energy levels. We have chosen to compare $(E_1+E_2)/2$ and $(E_3+E_4)/2$ so that the tunneling term is absent and a direct comparison with the simple harmonic oscillators can be made.

The agreement between this tight-binding approximation and the numerical calculations is good. We have also included the barrier height from one minimum to the other one in the same unit cell.

If we estimate the attempt frequency for t_1 as ω_m , then we find that for the parameters in Table I the action calculation gives $t_1 = 10^{-4}E_J$. From the full wave functions, we estimate $t_1 = (E_2 - E_1)/2 \approx 10^{-3}E_J$. This discrepancy can be made smaller by noting that in the calculation of the action, we could more accurately integrate from the classical turning points in the potential rather than from the minima.⁵⁵ However, for our purposes, the action expression will be sufficient for qualitative discussions, and we will use the full numerical calculations when estimating actual numbers.

So far we have estimated the energy levels and tunneling matrix elements when $f=1/2$. As f is decreased from $f=1/2$ the potential U changes such that one well becomes higher than the other, and the barrier height also changes. For the qubit we are mainly interested in the lowest two energy states of the system, so we now estimate the terms in tight-binding expression of Eq. (13). By defining the zero of energy as the average of the two lowest energy states at $f=1/2$, we find that the Hamiltonian for these two states is

$$H = \begin{pmatrix} F & -t \\ -t & -F \end{pmatrix}. \quad (22)$$

Here F is the energy change of each of the wells measured with respect to the energy of the wells at the degeneracy point; that is, $F = (\partial U / \partial f) \delta f$, where U is the potential energy. Note that since we will be operating the qubit just below the degeneracy point $f=1/2$, then $F < 0$. Also, $t = t_1 + \Delta t$, where t_1 is the intracell tunneling matrix element calculated at the degeneracy point and Δt is the change. The eigenvalues are $\lambda_{1,2} = \mp \sqrt{F^2 + t^2}$, where we have explicitly assumed that F is negative and t is positive.

The eigenvectors are given as the columns in the rotation matrix

$$D(\theta) = \begin{pmatrix} \cos \theta/2 & -\sin \theta/2 \\ \sin \theta/2 & \cos \theta/2 \end{pmatrix}, \quad (23)$$

where $\theta = -\arctan t/F$. For example, at the degeneracy point, $F=0$, so that $E = \mp t$ and the eigenvectors are $(1/\sqrt{2}, 1/\sqrt{2})^T$ and $(-1/\sqrt{2}, 1/\sqrt{2})^T$. These are just symmetric and antisymmetric combinations of the single well wave functions, as expected. For f slightly below $1/2$, we have $|F| \gg t$, so $\theta \approx 0$, and the energies are $E = \mp \sqrt{F^2 + t^2} \approx \pm F$. The eigenvectors are approximately $(1, 0)^T$ and $(0, 1)^T$, so that the eigenstates are nearly localized in each well.

It is more convenient to discuss the Hamiltonian and eigenstates in the rotated coordinate system such that $H_D = D^T(\theta) H D(\theta)$. In the rotated coordinate system, the Hamiltonian is diagonal with

$$H_D = -\sqrt{F^2 + t^2} \sigma_z, \quad (24)$$

and the eigenenergies are $E = \pm \sqrt{F^2 + t^2}$ and the eigenstates are then simply spin-down $|0\rangle = (1, 0)^T$ and spin-up $|1\rangle = (0, 1)^T$ vectors. In other words, no matter what the operating field is, we can always go to a diagonal representation; but the rotation matrix must be used to relate the simple spin-up and spin-down vectors to the linear combinations of the wave functions in the well.

V. MANIPULATION OF THE QUBIT

As noted above, the flexibility of the design of Josephson junction circuits affords a variety of methods for manipulating and controlling the state of qubits. In this section we show how the basic qubit circuit can be modified to allow precise control of its quantum states. To manipulate the states of the qubit, we need control over the properties of the qubit. For example, control over f , the magnetic field, allows one to change the operating point and F , the value of the energy difference between the two states. Control over the potential barrier height allows changing of the tunneling through t . For example, if the operating points of F_0 and t_0 are changed by ΔF and Δt , then the Hamiltonian in the rotated coordinate system is

$$H_D = -\sqrt{F_0^2 + t_0^2} \sigma_z + \Delta H_D, \quad (25)$$

where with $\theta_0 = -\arctan t_0/F_0$,

$$\Delta H_D = \Delta F (\cos \theta \sigma_z - \sin \theta \sigma_x) - \Delta t (\sin \theta \sigma_z + \cos \theta \sigma_x). \quad (26)$$

The control over F can be done by changing f . The control over t can be done by changing the barrier heights. To con-

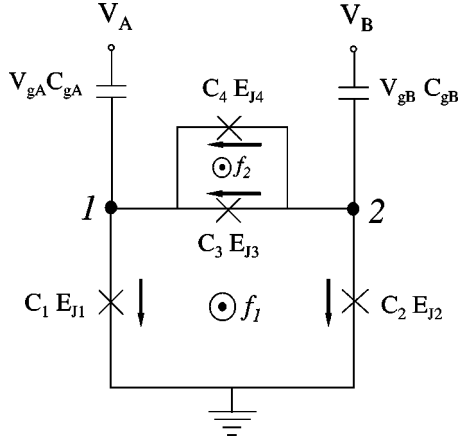


FIG. 6. The four-junction qubit. Two junctions form a SQUID loop and have Josephson energies and capacitance β times larger than the other junctions 1 and 2, which both have Josephson energies E_J and capacitance C . The nodes A and B represent the superconducting islands that are coupled by gate capacitors $C_g = \gamma C$ to gate voltages V_A and V_B . The arrows define the direction of the currents. The flux is out of the page.

control the barrier heights by external parameters, we replace the third junction by a SQUID, which acts like a variable strength junction. The modified circuit of the qubit is shown in Fig. 6.

We now analyze this circuit since it will be used in all subsequent discussion of the qubit. Flux quantization around each of the two loops gives $\varphi_1 - \varphi_2 + \varphi_3 = -2\pi f_1$ and $\varphi_4 - \varphi_3 = -2\pi f_2$. The Josephson energy due to each junction is $E_{Jn}(1 - \cos \varphi_n)$. The total Josephson energy U is then

$$\frac{U}{E_J} = 2 + 2\beta - 2 \cos \varphi_p \cos \varphi_m - 2\beta \cos(\pi f_a) \times \cos(2\pi f_b + 2\varphi_m), \quad (27)$$

where $\varphi_p = (\varphi_1 + \varphi_2)/2$ and $\varphi_m = (\varphi_1 - \varphi_2)/2$, and also $f_a = f_2$ and $f_b = f_1 + f_2/2$. Hence we see that $2\beta \cos(\pi f_a)$ plays the role of α in the three-junction qubit, but now this term can be changed by changing $f_a = f_2$, the flux in the top SQUID loop. Likewise, $f_b = f_1 + f_2/2$ plays the role of f in the three-junction qubit. The reduced Hamiltonian is then

$$H_t = \frac{1}{2} \frac{P_p^2}{M_p} + \frac{1}{2} \frac{P_m^2}{M_m} + E_J \{ 2 + 2\beta - 2 \cos \varphi_p \cos \varphi_m - 2\beta \cos(\pi f_a) \cos(2\pi f_b + 2\varphi_m) \}, \quad (28)$$

where $M_p = (\Phi_0/2\pi)^2 2C(1 + \gamma)$ and $M_m = (\Phi_0/2\pi)^2 2C(1 + 4\beta + \gamma)$.

To manipulate the parameters in the Hamiltonian let the magnetic fields change very slightly away from the some degeneracy point of f_1^* and f_2^* to a new operating point $f_1 = f_1^* + \epsilon_1$ and $f_2 = f_2^* + \epsilon_2$. Then F changes from zero to $F_0 = r_1 \epsilon_1 + r_2 \epsilon_2$ and t changes to $t_0 = t_1 + s_1 \epsilon_1 + s_2 \epsilon_2$, where r_i and s_i are constants and t_1 is the tunneling matrix element at the degeneracy point as found in the previous section. We take the operating point to be effectively in the regime where $f < 1/2$ in Fig. 4, so that $\epsilon_{1,2} < 0$. Hence, $F_0 < 0$. Also, t_0 is

assumed to remain positive. In the new rotated frame with $\theta_0 = -\arctan t_0/F_0$, the Hamiltonian given by Eq. (24) is $H_D = -\sqrt{F_0^2 + t_0^2} \sigma_z$.

Away from this new operating point, let $f_1 = f_1^0 + \delta_1$ and $f_2 = f_2^0 + \delta_2$. In the operation of the qubit, $|\delta_i| \ll |\epsilon_i|$ and δ_i usually will have a sinusoidal time dependence. Then $F = F_0 + r_1 \delta_1 + r_2 \delta_2$ and $t = t_0 + s_1 \delta_1 + s_2 \delta_2$, so that $\Delta F = r_1 \delta_1 + r_2 \delta_2$ and $\Delta t = s_1 \delta_1 + s_2 \delta_2$. Then the Hamiltonian in the rotated system with $\theta_0 = -\arctan t_0/F_0$ is

$$H_D = -\sqrt{F_0^2 + t_0^2} \sigma_z + \Delta H_D, \quad (29)$$

where

$$\Delta H_D = (r_1 \delta_1 + r_2 \delta_2) (\cos \theta_0 \sigma_z - \sin \theta_0 \sigma_x) - (s_1 \delta_1 + s_2 \delta_2) \times (\sin \theta_0 \sigma_z + \cos \theta_0 \sigma_x). \quad (30)$$

Hence we see that changes in the magnetic field from the operating point of f_1^0 and f_2^0 cause both σ_z and σ_x types of interactions.

To find the magnitude of these changes, we calculate the coefficients of change (r_1 , r_2 , s_1 and s_2) most simply at the degeneracy point where $\epsilon_i = 0$; that is, at the degeneracy point $f_i^0 = f_i^*$. We choose the degeneracy point for the four-junction qubit at $f_1^* = 1/3$ and $f_2^* = 1/3$. This results in classically doubly degenerate levels. In fact, any choice that satisfies $2f_1^* + f_2^* = 1$ when the classical energy U has two minima will also result in doubly degenerate levels. For example $f_1^* = 1/2$ and $f_2^* = 0$ is also a possible and convenient choice. However, we prefer $f_1^* = f_2^* = 1/3$ for the following reason. The change in potential energy with f_a gives

$$\frac{\partial U}{\partial f_a} = -2\pi\beta \sin \pi f_a \cos 2\varphi_m^0, \quad (31)$$

$$\frac{\partial^2 U}{\partial f_a^2} = -2\pi^2\beta \cos \pi f_a \cos 2\varphi_m^0.$$

The first order terms vanishes if $f_2^0 = 0$, resulting in the potential barrier always decreasing with changes in f_2 . On the other hand, if $f_2^0 = 1/3$, then the barrier height can be made to increase and decrease with changes in f_2 , thus allowing more control of the qubit.

Now the coefficients of change (r_1 , r_2 , s_1 , and s_2) can be estimated both from the numerical calculations and from the tight-binding model as shown in Appendix B. We find that at the degeneracy point of $f_1 = f_2 = 1/3$,

$$\frac{r_1}{E_J} = 2\pi \sqrt{1 - 1/(4\beta^2)}. \quad (32)$$

For our example with $\beta = 0.8$, we have $r_1/E_J = 4.90$. Estimates obtained from the numerical calculations done by changing f_1 and f_2 give $r_1/E_J = 4.8$ and $r_2/E_J = 2.4$ in good agreement with Eq. (B6) in Appendix B.

Likewise, from Appendix B we have that $s_1 = 0$ and $s_2 = \eta t \sqrt{E_J/E_c}$, where η is of the order of unity. For the operating point we find $\eta \sim 3.5$. Therefore, changes in H due to changes in t_1 go like σ_x . These tight-binding estimates for $\beta = 0.8$ give $s_1 = 0$ and $s_2/E_J = 0.03$. Full numerical calculations for our example give $s_1 = 0$ and $s_2/E_J = 0.20$. The

agreement with the tight-binding results are good, although the tight-binding underestimates s_2 for these parameters.

In summary, from the degeneracy point of $f_1^* = f_2^* = 1/3$, let the operating point be $f_1^0 = f_1^* + \epsilon_1$ and $f_2^0 = f_2^* + \epsilon_2$, so that $F_0 = r_1(\epsilon_1 \epsilon_2 / 2)$ and $t_0 = t_1 + s_2 \epsilon_2$. Now consider the changes in field about the operating point such that $f_1 = f_1^* + \delta_1$ and $f_2 = f_2^* + \delta_2$. In the rotated frame where $\theta_0 = -\arctan t_0 / F_0$, the Hamiltonian is

$$H_D = -\sqrt{F_0^2 + t_0^2} \sigma_z + \Delta H_D, \quad (33)$$

where

$$\begin{aligned} \Delta H_D = & r_1 \left(\delta_1 + \frac{\delta_2}{2} \right) (\cos \theta_0 \sigma_z - \sin \theta_0 \sigma_x) \\ & - s_2 \delta_2 (\sin \theta_0 \sigma_z + \cos \theta_0 \sigma_x), \end{aligned} \quad (34)$$

and $r_1 / E_J = 2\pi \sqrt{1 - 1/(4\beta^2)}$ and $s_2 = \eta t_0 \sqrt{E_J / E_c}$.

A typical design for a qubit will have $E_J / E_c = 80$, $\beta = 0.8$, $\gamma = 0.02$. We find from numerical calculations that $t_0 \approx 0.005 E_J$ and $\eta \approx 3.5$, which agree well with our tight-binding estimates. We operate at $f_1 = f_2 = 0.33$ so that $\epsilon_1 = \epsilon_2 = -1/300$. (This is equivalent to operating the three-junction qubit at $f = f_1 + f_2 / 2 = 0.495$ in Fig. 4.) Writing the energies as $E_i = h\nu_i$, we have taken typical values of $E_J = 200$ GHz and $E_c = 2.5$ GHz, and we find that $t_0 = 1$ GHz and $F_0 = 5$ GHz (which gives a splitting between the two states of about 10 GHz). The Hamiltonian is found to be

$$\frac{H_D}{E_J} = -0.025 \sigma_z + (4.0 \delta_1 + 2.1 \delta_2) \sigma_z - (0.46 \delta_1 + 0.41 \delta_2) \sigma_x. \quad (35)$$

The numerical values used are from numerical calculations. These values agree well with the estimates used in Eqs. (33) and (34) for the level splitting and the terms proportional to r_1 ; the terms proportional to s_2 match to about 50%, due to the more sensitive nature of estimating the tunneling terms.

The terms containing σ_x can be used to produce Rabi oscillations between the two states by modulating δ_1 and δ_2 with microwave pulses of the frequency of the level splitting of $2F_0 = 10$ GHz. One could arrange the values of δ_1 and δ_2 to make the time-varying σ_z term vanish. Then the operation of the qubit would be isomorphic to the NMR qubit. However, our simulations show that such an arrangement couples higher-energy levels and invalidates the simple two-state approximation. This is due to the large matrix element between the ground state and the second excited state given by the change in potential due to varying δ_2 . (It is interesting to note that similar coupling to higher levels occurs in qubits based on the rf SQUID and on simple charge states.) We propose to manipulate the qubit by varying δ_1 , which causes a Rabi oscillation through the σ_x term as well as a strong modulation of the Larmor precession through the time varying σ_z term. Because the Rabi frequency is much smaller than the Larmor frequency, the precession causes no problem for manipulating the qubit. For $\delta_1 = 0.001$ and $\delta_2 = 0$, the Rabi frequency is about 90 MHz. We note that this mode of operation is also possible with the three-junction qubit. Of course, it will not be possible to completely eliminate the

deleterious effects of the δ_2 coupling, but the effect of this coupling can be greatly reduced if δ_2 is restricted below 0.0001.

The varying magnetic fields δ_1 and δ_2 can be applied locally to the qubit by using a control line to inductively couple to the qubit. Moreover, if the control line is driven by a Josephson oscillator, then the coupling circuit could be fabricated on the same chip.

VI. INTERACTION BETWEEN QUBITS

A variety of methods is available for coupling qubits together. As noted in Refs. 13 and 14, essentially any interaction between qubits, combined with the ability to manipulate qubits individually, suffices to construct a universal quantum logic gate. Here we present two methods for coupling qubits inductively as shown in Fig. 7. The inductive coupling could either be permanent, or could be turned on and off at will by inserting Josephson junctions in the coupling loops.

Figure 7(a) shows one way of coupling two identical qubits. The lower portions of each qubit (the loops that contain the circulating currents) are inductively coupled.

To a first approximation we model the coupling as changing the flux in each of the two lower rings only through the mutual inductive coupling. (We ignore the self-inductance, which can easily be included.) The effective frustration in the lower loop of A, \tilde{f}_1^A , is changed over the applied frustration f_1^A to $\tilde{f}_1^A = f_1^A + M I_1^B / \Phi_0$. Here the current in the lower loop of B is I_1^B . Similarly, $\tilde{f}_1^B = f_1^B + M I_1^A / \Phi_0$. The coupled Hamiltonian is

$$H_{AB} = H^A(\tilde{f}_1^A) + H^B(\tilde{f}_1^B) + M I_1^A I_1^B, \quad (36)$$

which is the sum of the Hamiltonians for each system plus a term due to the mutual inductive coupling.

The inductively coupled contribution to the frustration is estimated to be of the order of $10^{-3} \Phi_0$ which is much smaller than the applied frustration. Since each persistent current will inductively couple into the other qubit, this will produce changes in the Hamiltonian of the σ_z and σ_x type and these changes will be proportional to the sign of the circulating currents in the qubit. Hence, we expect the coupling to be described by an interaction Hamiltonian of the form,

$$H_{AB}^{\text{int}} = \kappa_1 \sigma_z^A \sigma_z^B + \kappa_2 \sigma_z^A \sigma_x^B + \kappa_3 \sigma_x^A \sigma_z^B. \quad (37)$$

Hence we see that this interaction has both $\sigma_z^A \sigma_z^B$ and $\sigma_z^A \sigma_x^B$ types of coupling. We have estimated magnitude of $\kappa_i \approx 0.01 E_J$.

As Eq. (35) shows, the inductive coupling between the qubits can be made to be a substantial fraction of the qubit Larmor frequency. This is an attractive feature, as the coupling between two qubits sets the speed limit for how rapidly two qubit quantum logic operations can be performed in principle. In practice, it may be desirable to sacrifice speed of operation for enhanced accuracy: in this case, the inductive coupling could be designed to be smaller by decreasing the overlap of the inductive loops with the circuits.

Coupling between qubits is similar to the coupling we envision between the qubit and the measurement circuits

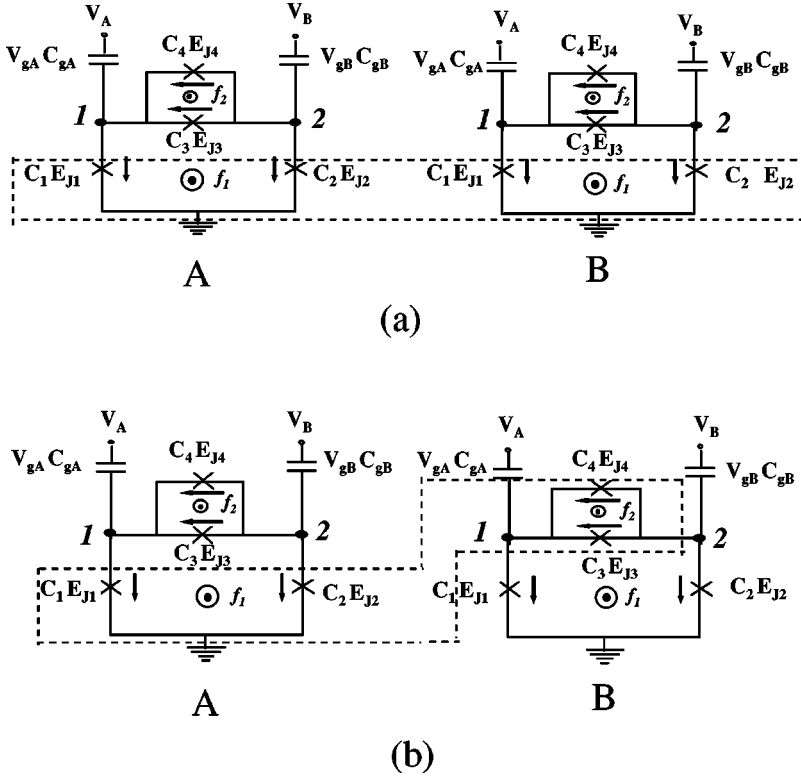


FIG. 7. Coupling of qubits A and B through the mutual inductance between (a) the lower regions of both, and (b) the lower region of A and the upper region of B.

containing SQUID-like detectors. In its usual configuration, the SQUID is biased in the voltage state that produces a voltage related to the flux through its detector loop. However, such a strong, continuous measurement on a qubit would destroy the superposition of states in the qubit and project out only one of the states. This problem can be circumvented by designing a SQUID such that it is current biased in the superconducting state and hence is not measuring the flux in its detector loop. When one needs to measure the qubit, the SQUID can be switched to its voltage state, for example, by applying a pulse of bias. The coupling from mutual inductance between the SQUID and the qubit will also have to be controlled. Other measurement schemes using SQUID's that are weakly coupled to the macroscopically coherent system have been proposed.⁵⁶

VII. COMPUTING WITH THE PC QUBIT

All the ingredients for quantum computation are now available. We have qubits that can be addressed, manipulated, coupled to each other, and read out. As will be indicated below, the particular qubits that we have chosen are well insulated from their environment as well. The flexibility of design for collections of qubits now allows a wide variety of overall designs for quantum computers constructed from such qubits.

Before discussing various superconducting quantum computer architectures, let us review some basic ideas about quantum logic and see how to implement quantum logic using our superconducting qubits. A quantum logic gate is a unitary operation on one or more qubits. Quantum computations are typically accomplished by building up quantum logic circuits out of many quantum logic gates. Just as in the case of classical computers, certain sets of quantum logic gates are universal in the sense that any quantum computa-

tion can be performed by wiring together members of the set. In fact, almost any interaction between two or more qubits is universal;^{13,14} but a convenient universal set of quantum logic gates widely used in the design of quantum algorithms consists of single qubit rotations and the quantum controlled-NOT gate, or CNOT.⁵⁷

A. One-qubit rotation

An arbitrary one qubit rotation can be written as $e^{-i\sigma t} = \cos t - i \sin t \sigma$ for some Pauli matrix $\sigma = a\sigma_x + b\sigma_y + c\sigma_z$, where $a^2 + b^2 + c^2 = 1$. There are many ways of accomplishing a one qubit rotation: the ability to rotate the qubit by a precise amount around any two orthogonal axes suffices. Pursuing the analog with NMR, we choose a method that involves applying an oscillatory field applied at the qubit's resonant frequency to rotate the qubit.

The Hamiltonian for a single qubit (A) can be gotten from Eq. (35). Here we assume $E_J = 200$ GHz, $\delta_1 = 0.001 \cos \omega t$ and $\delta_2 = 0$, and the level splitting is $\omega = 10$ GHz. Then, the Hamiltonian is

$$H_D(\text{GHz}) = 5\sigma_z + 0.80(\cos \omega t)\sigma_z - 0.09(\cos \omega t)\sigma_x. \quad (38)$$

The Rabi frequency is 90 MHz so that a π pulse would be about 20 nsec.

B. Two-qubit controlled NOT

A controlled NOT is a two qubit quantum logic gate that flips the value of the second qubit if the value of the first qubit is 1. That is, it takes $|00\rangle \rightarrow |00\rangle$, $|01\rangle \rightarrow |01\rangle$, $|10\rangle \rightarrow |11\rangle$, and $|11\rangle \rightarrow |10\rangle$. A controlled NOT can be combined with single qubit rotations to give arbitrary quantum logic operations. A controlled NOT can be straightforwardly imple-

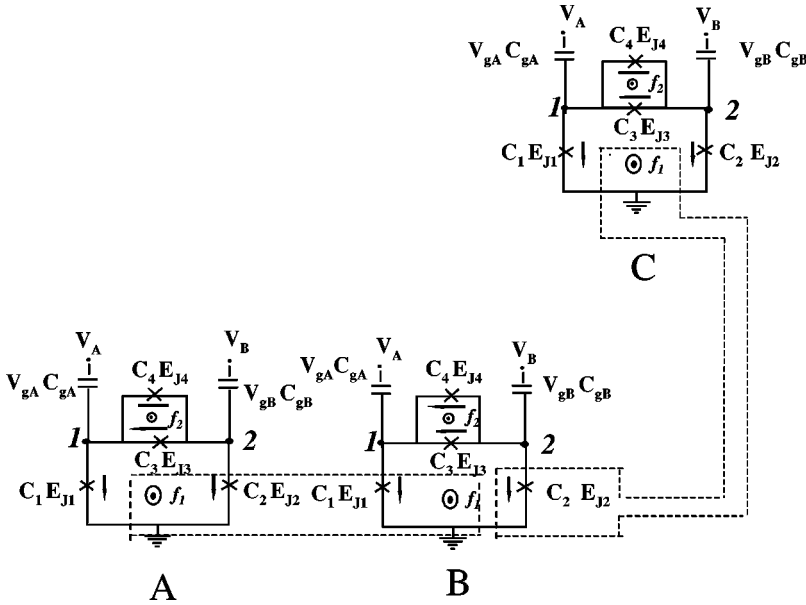


FIG. 8. A method for coupling a single qubit to other qubits.

mented in the superconducting qubit system by exploiting the analogy with NMR. Suppose that two qubits *A* and *B* have been constructed with an inductive coupling between their lower loops as in the first part of the previous section. Then the level splitting of qubit *B* depends on the state of qubit *A*, with values $\Delta E_{A,0}$ for *A* in the $|0\rangle$ state and $\Delta E_{A,1}$ for *A* in the $|1\rangle$ state. When a resonant pulse corresponding of $\Delta E_{A,1}/\hbar$ is applied to qubit *B*, it will only change if qubit *A* is in its $|1\rangle$ state. Since the coupling between the qubits is considerably larger than the Rabi frequency, the amount of time that it takes to perform the controlled NOT operation is equal to the amount of time it takes to perform a π rotation of a single qubit.

So the basic quantum logic operations can be performed on our superconducting qubits in a straightforward fashion. Accordingly, it is possible in principle to wire groups of qubits together to construct a quantum computer. A variety of architectures for quantum computers exist, usually consisting of regular arrays of quantum systems that can be made to interact either with their neighbors or with a quantum “bus” such as a cavity photon field or a phonon field in an ion trap that communicates equally with all the systems in the array. Because of the flexibility inherent in laying out the integrated Josephson junction circuit, a wide variety of architectures is possible. A particularly simple architecture for a quantum computer can be based on the proposal of Lloyd^{1,5} for arrays of quantum systems such as spins or quantum dots.

C. Linear chain of qubits

Consider a linear array of qubits $ABABABAB \dots$. Let the bottom of each qubit be inductively coupled to the top of the neighbor to the left. Also let each type of qubit, *A* and *B*, have a slightly different Josephson energy. Each qubit also has the area of the top loop which, is half that of the bottom loop. In the absence of the driving electromagnetic fluxes (the δ_i^j), the Hamiltonian for the system can be generalized to be written as

$$H = -\hbar \sum_k (\omega_k \sigma_k^z + 2J_{k,k+1} \sigma_k^z \sigma_{k+1}^z), \quad (39)$$

where $\hbar \omega_k = \sqrt{F_k^2 + t_k^2}$ and $J_{k,k+1} = \kappa_{k,k+1}(r_{1,k} + r_{1,k+1})/2$. This problem then maps on the linear chain of nuclear spins that was shown by Lloyd⁵ to be a universal quantum computer. The coupling needed to perform $\pi/2$ pulses is provided by the terms containing the δ_i^j 's. The nice feature of this linear chain is that separate control lines for ac fields are not needed. The whole linear array can sit in a microwave cavity and be pulsed at the desired frequency. (The dc bias fields to ensure $f_1 = f_2 = 1/3$ will require at least two dc control lines.) The frequencies needed are around 10–25 GHz with intervals of 1 GHz (and with resolution of about 0.1 GHz). We could make these numbers larger or smaller if needed.

Details of computing with this are given in various references, see, for examples, Ref. 5 and Chap. 20 of Ref. 58.

D. Superconducting quantum integrated circuits

There is no reason why the inductive loops cannot couple qubits that are far apart. In addition, a single qubit can be coupled to several other qubits as shown in Fig. 8.

This arrangement requires separate ac control lines for each of the qubits, which then demands localized on-chip oscillators. One can build up essentially arbitrary integrated circuits of superconducting qubits by this method. This flexibility in the construction of quantum computer architectures is one of the benefits of using superconducting Josephson junction circuits to perform quantum computation. The quantum integrated circuit could be set up to provide a number of useful features. For example,⁵⁹ one might be able to design the circuit and interactions in such a way that it automatically implements an intrinsically fault-tolerant quantum computer architecture such as those proposed by Kitaev⁶⁰ and Preskill.⁶¹ In addition, since the circuits are parallelizable in that different quantum logic operations can be performed in different places simultaneously, the circuit could be designed to provide the maximum possible parallelization of a particular problem such as factoring,⁶² database search,⁶³ or computing a discrete quantum Fourier transform.^{62,64}

VIII. DECOHERENCE

We have shown how superconducting circuits can be used to construct qubits and quantum logic circuits. These superconducting qubits have been idealized in the sense that we have ignored the effects of manufacturing variability, noise, and decoherence. Manufacturing variability can be compensated for as discussed above: before performing any quantum computations, the properties of individual qubits can be measured, recorded in a look-up table in a conventional computer, and used either to supply compensating calibration fields or to alter the frequencies with which control pulses are supplied to the qubits.

From the point of view of the ultimate performance of a superconducting computer, a more pressing issue is that of environmentally induced noise and decoherence. In real systems the performance of a qubit will be limited by dissipative mechanisms that cause the quantum state to decohere in time τ_d . The ‘‘quality factor’’ for a qubit is the decoherence time divided by the amount of time it takes to perform fundamental quantum logic operations.³ The quality factor gives the number of quantum logic operations that can be performed before the computation decoheres, and should be 10^4 or greater for the quantum computer to be able to perform arbitrarily long quantum computations by the use of error-correction techniques.^{65–69}

Decoherence can be due to ‘‘internal’’ dissipation (quasiparticle resistance), or coupling to an environmental degree of freedom. It is also possible to couple to an environmental degree of freedom, without a dissipative mechanism, that will still lead to decoherence.⁷⁰

We will now discuss some of the major sources of decoherence.

Normal state quasiparticles can cause dissipation and energy relaxation at finite temperatures in Josephson junctions. However, mesoscopic aluminum junctions have been shown to have the BCS temperature dependence for the density of quasiparticles. At low temperatures this density is exponentially small,⁷¹ so quasiparticle tunneling will be strongly suppressed at low temperatures and at low voltages, as was seen in a system with multiple superconducting islands in Ref. 72. We estimate a lower bound of 10^4 for the quality factor, given a subgap resistance of $10^{10}\Omega$.⁷¹

The qubit can also decohere by spontaneous emission of photons. We estimate this effect for the case of emission into free space. From the example considered below we conclude that it is advantageous to have the typical size of the system (the dipole moment dimensions) much smaller than the radiated wavelength, so that the qubit is a maximally inefficient antenna.

We start with a classical expression for the magnetic dipole radiation from an oscillating current in the qubit loop, and use it for estimating the emission rate of photons. (For the treatment of a more general problem of damping by a dissipative electromagnetic environment, see Ref. 73.) For a loop of radius R with an oscillating current of the amplitude of I_m , the radiated power is $P_m = \frac{4}{3}\pi^5 I_m^2 Z_0 (R/\lambda)^4$. Here Z_0 is the vacuum impedance and $\lambda = c/\nu$ is the wavelength of radiation at the oscillation frequency ν . The radiation is small when the qubit size R is much smaller than λ . A typical rate for photon emission is $t_m^{-1} = P_m/h\nu$, which gives an es-

timate of the decoherence time of $t_m = 3hc^4/(4\pi^5 I_m^2 Z_0 R^4 \nu^3)$. Here the frequency is taken to be the Larmor frequency (other characteristic frequencies such as the Rabi frequency are even smaller). For our qubit $R \approx 1 \mu\text{m}$, $\nu \approx 10 \text{ GHz}$, and $\lambda = 3 \text{ cm}$. The amplitude I_m is the oscillating part of $\langle \Psi(t) | I_C \sin\varphi_1 | \Psi(t) \rangle \approx \langle \Psi_1 | I_C \sin\varphi_1 | \Psi_2 \rangle = 1 \text{ nA}$, where $\Psi(t)$ is an arbitrary superposition of the two eigenstates $\Psi_{1,2}$. Note that $I_m \ll I_C$ since we operate the qubit away from the degeneracy point, so that the eigenstates strongly overlap with the pure Josephson current states.

Using these numbers we find that $t_m \sim 10^7$ sec, so that the radiation is not a serious source of decoherence. We checked that dipole radiation from electric dipole moments is even weaker for our system. However, it should be noted that some proposals for using rf SQUID’s for qubits involve oscillating currents of the order of $1 \mu\text{A}$ and loops of the order of $10 \mu\text{m}$. These rf SQUID’s have $t_m \approx 10^{-3}$ sec, which is substantially lower than for our qubit which can be made much smaller and operate at much less current.

Inhomogeneity in the magnetic flux distribution can also be a source of decoherence. This is similar to T_2 in NMR systems. We estimate this for our system by calculating the amount of flux a $1 \mu\text{m} \times 1 \mu\text{m}$ wire carrying 100 nA of current induces in a loop of the same size which has its center $3 \mu\text{m}$ away. We find that the induced frustration is about $\delta f = 10^{-7}$. If this is taken as an estimate of the typical variance of the frustration that difference qubits experience, then there will be a spread of operating frequencies among the loops. An estimate of t_d is the time for the extremes of this frequency differ by π . This results in $t_d \approx \pi/(2r_1 \delta f)$, where we have taken the larger value from Eq. (35). With $r_1/\hbar \approx 600 \text{ GHz}$, we find $t_d \approx 1.5 \text{ msec}$. The dipole-dipole interaction between qubits gives a time of the same order.

We have also estimated the magnetic coupling between the dipole moment of the current loops and the magnetic moments of the aluminum nuclei in the wire. At low temperatures where the quasiparticles are frozen out, the decoherence time for a single qubit is of the order of T_1 , which is exponentially large in the low-temperature superconducting state. For an ensemble of qubits, the decoherence time may be of the order of milliseconds due to the different configurations of nuclear spins in the different qubits. However, this effect may be reduced by aligning the spins or by applying compensating pulse sequences.

Coupling to Ohmic dissipation in the environment has been modeled for superconducting qubits operating in the charging regime.¹⁹ In this case, the source of decoherence can be made sufficiently small such that the quality factor is large enough. Similar calculations for qubits in the superconducting regime of circulating currents have not yet been done. Experiments to measure this decoherence time in our circuits are underway. In practice electromagnetic coupling to the normal state ground plane can limit coherence,³⁵ however, a superconducting ground plane can greatly reduce this coupling.

Other possible sources of decoherence are the effects of the measuring circuit, the arrangement and stability of the control lines for the magnetic fields, and the ac dielectric losses in the substrate at microwave frequencies. These and other source of decoherence will have to be estimated in a real circuit environment and measured.

Taking 0.1 msec as a lower bound on the decoherence time and 10 nsec as a switching time, we find that the quality factor is of the order of 10^4 . Furthermore, if the proper set of topological excitations is used to store information, the decoherence time for quantum computation can be made substantially longer than the minimum decoherence time for an individual junction circuit.⁶⁰

IX. SUMMARY

In this paper we have discussed a superconducting qubit that has circulating currents of opposite sign as its two logic states. The circuit consist of three nanoscale Josephson junctions connected in a superconducting loop and controlled by magnetic fields. One of the three junctions is a variable junction made as a SQUID loop. This qubit has quantum states which are equivalent to the states of a particle with an anisotropic mass moving in an two-dimensional periodic potential. Numerical calculations of the quantum states of the qubit have been made as well as physical estimates from a tight-binding approximation. The advantages of this qubit is that it can be made insensitive to background charges in the substrate, the flux in the two states can be detected, and the states can be manipulated with magnetic fields. Coupled systems of qubits are also discussed as well as sources of decoherence.

ACKNOWLEDGMENTS

This work was supported by ARO Grant No. DAAG55-98-1-0369. T.P.O. acknowledges support from the Technical University of Delft and the Center for Superconductivity at the University of Maryland, where part of this work was done. J.J.M. was supported by the Fulbright Fellowship and from DGES (PB95-0797). The work in Delft was financially supported by the Dutch Foundation for Fundamental Research on Matter (FOM). We thank Kostya Likharev, Kees Harmans, Peter Hadley, Chris Lobb, Fred Wellstood, and Ton Wallast for stimulating and useful discussions.

APPENDIX A: CLASSICAL STABILITY

In this appendix we find the eigenvalues of the stability matrix for the three-junction potential and the range of frustration around $f=1/2$, where there are two stable classical solutions with opposite circulating currents.

The potential energy of the Josephson energy of the three-junction qubit is given by Eq. (1),

$$\tilde{U} = \frac{U}{E_J} = 2 + \alpha - \cos \varphi_1 - \cos \varphi_2 - \alpha \cos(2\pi f + \varphi_1 - \varphi_2). \quad (\text{A1})$$

We are interested in minimum energy phase configurations; that is, stable solutions of the following system of equations:

$$\begin{aligned} \frac{\partial \tilde{U}}{\partial \varphi_1} &= \sin \varphi_1 + \alpha \sin(2\pi f + \varphi_1 - \varphi_2) = 0, \\ \frac{\partial \tilde{U}}{\partial \varphi_2} &= \sin \varphi_2 - \alpha \sin(2\pi f + \varphi_1 - \varphi_2) = 0. \end{aligned} \quad (\text{A2})$$

The solutions $(\varphi_1^*, \varphi_2^*)$ comply with $\sin \varphi_1^* = -\sin \varphi_2^* = \sin \varphi^*$. Then

$$\sin \varphi^* = -\alpha \sin(2\pi f + 2\varphi^*). \quad (\text{A3})$$

In order to check the character of the solution we compute the eigenvalues of the stability matrix, $\partial^2 \tilde{U} / \partial \varphi_i \partial \varphi_j$, where

$$\begin{aligned} \frac{\partial^2 \tilde{U}}{\partial \varphi_1^2} &= \cos \varphi_1 + \alpha \cos(2\pi f + \varphi_1 - \varphi_2), \\ \frac{\partial^2 \tilde{U}}{\partial \varphi_2^2} &= \cos \varphi_2 + \alpha \cos(2\pi f + \varphi_1 - \varphi_2), \end{aligned} \quad (\text{A4})$$

$$\frac{\partial^2 \tilde{U}}{\partial \varphi_1 \partial \varphi_2} = -\alpha \cos(2\pi f + \varphi_1 - \varphi_2).$$

For the states with $\cos \varphi_1^* = \cos \varphi_2^* = \cos \varphi^*$ (these are the ones we are interested here), the eigenvalues are

$$\lambda_1 = \cos \varphi^*,$$

$$\lambda_2 = \cos \varphi^* + 2\alpha \cos(2\pi f + 2\varphi^*). \quad (\text{A5})$$

When $f \neq 0, 1/2$ we have used relaxation methods for computing φ^* . Both eigenvalues are greater than zero, which assures the minimum energy condition. Figure 2 shows the energy of the minimum energy configurations for $\alpha=0.8$. We find that there exists a region of values of the field for which two different minimum energy phase configurations coexist.

Next we calculate the critical values of the external field for this coexistence. We can restrict our analysis to the region around $f=0.5$; that is, $[0.5 - f_c, 0.5 + f_c]$ (where $f_c \geq 0$). These extrema values of the field correspond to solutions for which one of the eigenvalues is positive and the other equals zero. The inset of Fig. 2 shows $f_c(\alpha)$.

We first calculate f_c when $\alpha \geq 1.0$. The first eigenvalue that equals zero is λ_1 . Then at $f=0.5 \pm f_c$, $\lambda_1=0$ which implies $\varphi^* = \mp \pi/2 \pmod{2\pi}$ (here and below we associate the sign in f_c with the sign of the phase in order to have $f_c \geq 0$). Then, going to Eq. (A3) we get

$$\begin{aligned} \sin(\mp \pi/2) &= -\alpha \sin(\pi \pm 2\pi f_c \mp \pi), \\ \pm 1 &= \pm \alpha \sin(2\pi f_c) \end{aligned} \quad (\text{A6})$$

and

$$f_c = \frac{1}{2\pi} \arcsin \frac{1}{\alpha}. \quad (\text{A7})$$

We now calculate f_c when $0.5 \leq \alpha \leq 1.0$. Now the first eigenvalue to equal zero is λ_2 , and we have to solve

$$\begin{aligned} \sin \varphi^* &= -\alpha \sin(2\pi f + 2\varphi^*) = \alpha \sin(\pm 2\pi f_c + 2\varphi^*), \\ \cos \varphi^* &= -2\alpha \cos(2\pi f + 2\varphi^*) = 2\alpha \cos(\pm 2\pi f_c + 2\varphi^*). \end{aligned} \quad (\text{A8})$$

We will use $\Delta = \pm 2\pi f + 2\varphi^*$, so that

$$\begin{aligned}
1 &= \sin^2 \varphi^* + \cos^2 \varphi^* \\
&= \alpha^2 \sin^2 \Delta + 4\alpha^2 \cos^2 \Delta \\
&= \alpha^2 + 3\alpha^2 \cos^2 \Delta.
\end{aligned} \tag{A9}$$

Then

$$\begin{aligned}
\cos \Delta &= \sqrt{\frac{1-\alpha^2}{3\alpha^2}}, \quad \Delta = \mp \arccos\left(\sqrt{\frac{1-\alpha^2}{3\alpha^2}}\right) \\
\cos \varphi^* &= 2\sqrt{\frac{1-\alpha^2}{3}}\varphi^* = \mp \arccos\left(2\sqrt{\frac{1-\alpha^2}{3}}\right).
\end{aligned} \tag{A10}$$

Here we have followed the solution corresponding to $\cos(\varphi^*) \geq 0$. Finally we have the solution for f_c ($\Delta = \pm 2\pi f_c + 2\varphi^*$),

$$f_c = \frac{1}{2\pi} \left[2\arccos\left(2\sqrt{\frac{1-\alpha^2}{3}}\right) - \arccos\left(\sqrt{\frac{1-\alpha^2}{3\alpha^2}}\right) \right]. \tag{A11}$$

APPENDIX B: TIGHT-BINDING ESTIMATE OF COEFFICIENTS OF CHANGE

Recall that $f_a = f_2$ and $f_b = f_1 + f_2/2$. Assume that we change f_a and f_b independently. The minima in U occur at $\varphi_p^* = 0$ and $\varphi_m^* = \pm \varphi_m^0$. Therefore, the energy due to the potential energy is for each of the minimum

$$\frac{U}{E_J} = 2 + 2\beta - 2\cos\varphi_m^* - 2\beta\cos(\pi f_a)\cos(2\pi f_b + 2\varphi_m^*). \tag{B1}$$

The change in the magnetic flux f_a by δf_a causes a change in U of

$$\frac{\partial U}{\delta f_a} \delta f_a = -2\pi\beta \sin \pi f_a \cos 2\varphi_m^0 \delta f_a, \tag{B2}$$

which is the same for the minimum at $\pm \varphi_m^0$. Whereas, the flux f_b causes a change

$$\frac{\partial U}{\delta f_b} \delta f_b = \mp 4\pi\beta \cos \pi f_a \sin 2\varphi_m^0 \delta f_b, \tag{B3}$$

which has opposite signs for the two minimum. Therefore,

$$\begin{aligned}
\frac{\Delta U}{E_J} &= -2\pi\beta \sin \pi f_a \cos 2\varphi_m^0 \delta f_a \mathbf{1} \\
&\quad - 4\pi\beta \cos \pi f_a \sin 2\varphi_m^0 \delta f_b \sigma_z.
\end{aligned} \tag{B4}$$

Recall that ΔF in the change is the energy between the two states when there is no tunneling. This is the second term in Eq. (B4), since the first term is only a constant for both levels, so that

$$\frac{\Delta F}{E_J} = -4\pi\beta \cos \pi f_a \sin 2\varphi_m^0 \delta f_b \sigma_z. \tag{B5}$$

For this change $\Delta F = r_1 \delta_1 + r_2 \delta_2$; and since $\delta f_b = \delta_1 + \delta_2/2$, we have $r_1 = 2r_2$ and

$$\frac{r_1}{E_J} = 4\pi\beta \cos \pi f_a \sin 2\varphi_m^0. \tag{B6}$$

We have found previously that $\cos \varphi_m^0 = 1/2\alpha$ where $\alpha = 2\beta \cos \pi f_a$ so that with $f_a = 1/3$,

$$\frac{r_1}{E_J} = 2\pi\sqrt{1 - 1/(4\beta^2)}. \tag{B7}$$

To find the changes in Δt , we see that the changes in $t_1 = (\hbar \omega_m / 2\pi) e^{-S_1/\hbar}$ are dominated by changes in S_1 , so that

$$\Delta t = -\frac{t}{\hbar} \sum_{i=a,b} \frac{\partial S_1}{\partial f_i} \delta f_i. \tag{B8}$$

The changes in f_b do not change S_1 to first order. Hence, changes in t come from changes in $f_a = f_2$ only, so that $s_1 = 0$. But changes in f_a are equivalent to changes in α in the three-junction problem, so we can use Eqs. (B8) and (16) and the fact that $2\beta \cos(\pi f_a)$ plays the role of α to find

$$\Delta t = \frac{\pi t}{\hbar} \frac{\partial S_1}{\partial \alpha} (2\beta \sin \pi f_a) \delta f_a. \tag{B9}$$

This allows us to write $s_2 = \eta t \sqrt{E_J/E_c}$, where η is of the order of unity. For the operating point we find $\eta \sim 3.5$. Therefore, changes in H due to changes in t_1 go like σ_x . These tight-binding estimates for $\beta = 0.8$ and $f_a = 1/3$ give $s_1 = 0$ and $s_2 = 0.03$.

¹S. Lloyd, Science **261**, 1589 (1993).

²C.H. Bennett, Phys. Today **48** (10), 24 (1995).

³D.P. DiVincenzo, Science **269**, 225 (1995).

⁴T.P. Spiller, Proc. IEEE **84**, 1719 (1996).

⁵S. Lloyd, Sci. Am. **273**, 140 (1995).

⁶B. Schumacher, Phys. Rev. A **51**, 2738 (1995).

⁷S. Lloyd, Science **263**, 695 (1994).

⁸R. Landauer, Int. J. Theor. Phys. **21**, 283 (1982); Found. Phys. **16**, 551 (1986); Nature (London) **335**, 779 (1988); *Nanostructure Physics and Fabrication*, edited by M. A. Reed and W. P. Kirk (Academic, Press Boston, 1989), p. 17–29; Phys. Today **42**(10), 119 (1989); Phys. Today **44** (5), 23 (1991); *Proceedings of the*

Workshop on Physics of Computation II, edited by D. Matzke (IEEE Press, Los Alamitos, CA, 1992).

⁹Q.A. Turchette, C.J. Hood, W. Lange, H. Mabuchi, and H.J. Kimble, Phys. Rev. Lett. **75**, 4710 (1995).

¹⁰C. Monroe, D.M. Meekhof, B.E. King, W.M. Itano, and D.J. Wineland, Phys. Rev. Lett. **75**, 4714 (1995).

¹¹N.A. Gershenfeld and I.L. Chang, Science **275**, 350 (1997).

¹²D. G. Cory, A. F. Fahmy, and T. F. Havel, *Proceedings of the Fourth Workshop on Physics and Computation*, edited by T. Toffoli, M. Biafore, and J. Leao (New England Complex Systems Institute, Boston, 1996), pp. 87–91.

¹³S. Lloyd, Phys. Rev. Lett. **75**, 346 (1995).

- ¹⁴D. Deutsch, A. Barenco, and A. Ekert, Proc. R. Soc. London, Ser. A **449**, 669 (1995).
- ¹⁵B.E. Kane, Nature (London) **393**, 133 (1998).
- ¹⁶J. E. Mooij, *Conference on Quantum Coherence and Decoherence, Santa Barbara, California, 1996* (Royal Soc. of London, London, 1998).
- ¹⁷J. E. Mooij, T. P. Orlando, L. Levitov, Lin Tian, Caspar H. van der Wal, and Seth Lloyd, Science (to be published).
- ¹⁸M.F. Bocko, A.M. Herr, and M.F. Feldman, IEEE Trans. Appl. Supercond. **7**, 3638 (1997).
- ¹⁹A. Shnirman, G. Schön, and Z. Hermon, Phys. Rev. Lett. **79**, 2371 (1997).
- ²⁰D.V. Averin, Solid State Commun. **105**, 659 (1998).
- ²¹N. P. Suh, *The Principles of Design* (Oxford University Press, Oxford, 1990).
- ²²M. Tinkham, *Introduction to Superconductivity*, 2nd ed. (McGraw-Hill, New York, 1996).
- ²³*Single Charge Tunneling*, edited by H. Grabert and M. Devoret (Plenum, New York, 1992).
- ²⁴P. Carruthers and M.M. Nieto, Rev. Mod. Phys. **40**, 411 (1968).
- ²⁵P. Joyez, A. Pilipe, D. Esteve, and M.H. Devoret, Phys. Rev. Lett. **72**, 2458 (1994).
- ²⁶M. Matters, W.J. Elion, and J.E. Mooij, Phys. Rev. Lett. **75**, 721 (1995).
- ²⁷V. Bouchiat, D. Vion, P. Joyez, D. Esteve, and M. Devoret, Phys. Scr. **T76**, 165 (1998); V. Bouchiat, Ph.D. thesis, Université Paris, 1997.
- ²⁸D. V. Averin and K. K. Likharev, in *Mesoscopic Phenomena in Solids*, edited by B. L. Altshuler, P. A. Lee, and R. A. Webb (North-Holland, Amsterdam, 1991).
- ²⁹P. Lafarge, M. Matters, and J.E. Mooij, Phys. Rev. B **54**, 7380 (1996).
- ³⁰W.J. Elion, M. Matters, U. Geigenmüller, and J.E. Mooij, Nature (London) **371**, 594 (1994).
- ³¹A. van Oudenaarden, S.J.K. Vårdy, and J.E. Mooij, Czech. J. Phys. **46**, 707 (1996).
- ³²L.J. Geerligs, V.F. Anderegg, and J.E. Mooij, Physica B **165**, 973 (1990).
- ³³G. Zimmerli, T.M. Eiles, R.L. Kautz, and John M. Martinis, Appl. Phys. Lett. **61**, 237 (1992).
- ³⁴S. Han, J. Lapointe, J. E. Lukens, in *Activated Barrier Crossing*, edited by G. R. Fleming and P. Hanggi (World Scientific, Singapore, 1993), pp. 241–267.
- ³⁵R. Rouse, S. Han, and J.E. Lukens, Phys. Rev. Lett. **75**, 1614 (1995).
- ³⁶J. Diggins, T.D. Clark, H. Prance, R.J. Prance, T.P. Spiller, J. Ralph, and F. Brouers, Physica B **215**, 367 (1995).
- ³⁷M.G. Castellano, R. Leoni, and G. Torrioli, J. Appl. Phys. **80**, 2922 (1996).
- ³⁸T. P. Orlando and K. A. Delin, *Introduction to Applied Superconductivity* (Addison and Wesley, Reading, MA, 1991).
- ³⁹S. Doniach, in *Percolation, Localization, and Superconductivity*, Vol. 109 of *NATO Advanced Study Institute, Series B: Physics*, edited by A. M. Goldman and S. A. Wolf (Plenum, New York, 1984), p. 401.
- ⁴⁰In fact, Likharev has pointed out that replacing the third junction by an inductor also will give a similar functional form for U . We choose the three junction system instead because the inductor values needed are not as accessible with our technology. We have also carried out quantum-mechanical simulations with the inductor and do indeed find that it has similar properties to what is reported here.
- ⁴¹D. A. Wells, *Theory and Problems of Lagrangian Dynamics* (McGraw-Hill, New York, 1967), Chap. 15.
- ⁴²D. C. White and H. H. Woodson, *Electromechanical Energy Conversion* (Wiley, New York, 1959), Chap. 1.
- ⁴³M. H. Devoret, in *Quantum Fluctuations*, edited by S. Reymaud, E. Giacobino, and J. Zinn-Justin (Elsevier, New York, 1997), Chap. 10.
- ⁴⁴T. P. Orlando *et al.* (unpublished).
- ⁴⁵S. P. Yukon and N.C. H. Lin, *Macroscopic Quantum Phenomena and Coherence in Superconducting Networks* (World Scientific, Singapore, 1995), p. 351; IEEE Trans. Appl. Supercond. **5**, 2959 (1995).
- ⁴⁶U. Geigenmüller, J. Appl. Phys. **80**, 3934 (1996).
- ⁴⁷M. Barahona, E. Trías, T.P. Orlando, A.E. Duwel, H.S.J. van der Zant, S. Watanabe, and S.H. Strogatz, Phys. Rev. B **55**, 11 989 (1997).
- ⁴⁸P. Caputo, A. E. Duwel, T. P. Orlando, A. V. Ustinov, N. C. H. Lin, and S. P. Yukon (unpublished).
- ⁴⁹G. Schön and A.D. Zaikin, Physica B **152**, 203 (1988).
- ⁵⁰T. P. Spiller, T. D. Clark, R. J. Prance, and A. Widom, in *Progress in Low Temperature Physics*, edited by D. F. Brewer (Elsevier, New York, 1992), Vol. XIII, Chap. 4.
- ⁵¹K.K. Likharev and A.B. Zorin, J. Low Temp. Phys. **59**, 347 (1985).
- ⁵²E.U. Condon, Phys. Rev. **31**, 891 (1928).
- ⁵³Note that H_i could have been found directly by not making the Legendre transformation in the Lagrangian. Then the canonical momentum would not be proportional to the charges on the nodes. Although this canonical momentum and Hamiltonian are clearer mathematically, we use instead the more physical canonical momentum which is proportional to the charge so as to make better contact with the literature, such as in Refs. 43, 49, and 50.
- ⁵⁴H.S.J. van der Zant, D. Berman, T.P. Orlando, and K.A. Delin, Phys. Rev. B **49**, 12 945 (1994).
- ⁵⁵L. D. Landau and E. M. Lifshitz, *Quantum Mechanics*, 3rd ed. (Pergamon, New York, 1977), Vol. 3, pp. 183–184.
- ⁵⁶C.D. Tesche, Physica B **165&166**, 925 (1990); Also Jpn. J. Appl. Phys., Suppl. **26**, 1409 (1987).
- ⁵⁷A. Barenco, C.H. Bennett, R. Cleve, D.P. DiVincenzo, N. Margolus, P. Shor, T. Sleator, J.A. Smolin, and H. Weinfurter, Phys. Rev. A **52**, 3457 (1995).
- ⁵⁸G. P. Berman, G. D. Doolen, and R. Mainieri, *Introduction to Quantum Computers* (World Scientific, Singapore, 1998).
- ⁵⁹C. Ahn, S. Lloyd, and B. Rahn (unpublished).
- ⁶⁰A.Y. Kitaev, quant-ph/9707021 (unpublished).
- ⁶¹J. Preskill, quant-ph/9712048 (unpublished).
- ⁶²P. Shor, in *Proceedings of the 35th Annual Symposium on Foundations of Computer Science*, edited by S. Goldwasser (IEEE Computer Society, Los Alamitos, CA, 1994), pp. 124–134.
- ⁶³L.K. Grover, Phys. Rev. Lett. **79**, 325 (1997).
- ⁶⁴D. R. Simon, in *Proceedings of the 35th Annual Symposium on Foundations of Computer Science* (Ref. 62), pp. 116–123.
- ⁶⁵P. Shor, in *Proceedings of the 37th Annual Symposium on the Foundations of Computer Science* (IEEE Computer Society Press, Los Alamitos, 1996), pp. 56–65.
- ⁶⁶A. Steane, Proc. R. Soc. London, Ser. A **452**, 2551 (1996).
- ⁶⁷D.P. DiVincenzo and P.W. Shor, Phys. Rev. Lett. **77**, 3260 (1996).

- ⁶⁸J.I. Cirac, T. Pellizzari, and P. Zoller, *Science* **273**, 1207 (1996).
- ⁶⁹E. Knill and R. Laflamme, *Phys. Rev. A* **55**, 900 (1997).
- ⁷⁰A. Stern, Y. Aharonov and Y. Imry, *Phys. Rev. A* **41**, 3436 (1990).
- ⁷¹C.D. Tesche, *Phys. Rev. Lett.* **64**, 2358 (1990); also, Johnson and M. Tinkham, *ibid.* **65**, 1263 (1990).
- ⁷²Caspar H. van der Wal and J. E. Mooij, *J. Superconductivity* (to be published).
- ⁷³A. J. Leggett, S. Chakravarty, A. T. Dorsey, M. P. A. Fisher, A. Garg, and W. Zwerger, *Rev. Mod. Phys.* **59**, 1 (1987).
- ⁷⁴C. Kittel, *Introduction to Solid State Physics* (Wiley, New York, 1974), Chap. 9.